

## Structural Basis of Noscopine Activation for Tubulin Binding

María A. Oliva,<sup>¶</sup> Andrea E. Prota,<sup>¶</sup> Javier Rodríguez-Salarichs,<sup>¶</sup> Youssef L. Bennani, Jesús Jiménez-Barbero, Katja Bargsten, Angeles Canales, Michel O. Steinmetz, and J. Fernando Díaz\*Cite This: *J. Med. Chem.* 2020, 63, 8495–8501

Read Online

ACCESS |



Metrics &amp; More

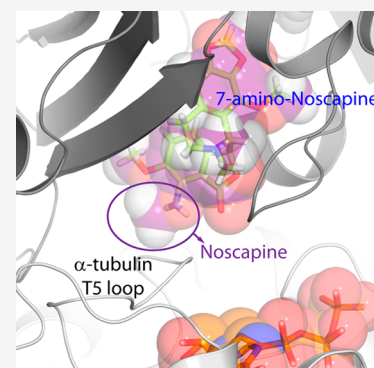


Article Recommendations



Supporting Information

**ABSTRACT:** Noscopine is a natural alkaloid that is used as an antitussive medicine. However, it also acts as a weak anticancer agent in certain *in vivo* models through a mechanism that is largely unknown. Here, we performed structural studies and show that the cytotoxic agent 7A-*O*-demethoxy-amino-noscopine (7A-aminonoscopine) binds to the colchicine site of tubulin. We suggest that the 7A-methoxy group of noscopine prevents binding to tubulin due to a steric clash of the compound with the T5-loop of  $\alpha$ -tubulin. We further propose that the anticancer activity of noscopine arises from a bioactive metabolite that binds to the colchicine site of tubulin to induce mitotic arrest through a microtubule cytoskeleton-based mechanism.



## INTRODUCTION

Among systemic and wide spectrum anticancer chemotherapies, those directed against tubulin have shown to be extremely successful. Vinca drugs discovered in the 60's were the first magic bullet against leukemia,<sup>1</sup> while taxanes became in the 90's the best choice for the treatment of solid tumors (breast, ovarian, prostatic, lung).<sup>2</sup> More recently, high affinity drugs targeting the vinblastine site on  $\beta$ -tubulin (e.g., auristatin) or the newly discovered maytansine site<sup>3</sup> had shown excellent activity as antibody drug conjugates.<sup>4</sup> Finally, newly developed chemotypes with improved properties targeting the vinca (eribulin)<sup>5</sup> or the taxane (ixabepilone)<sup>6</sup> sites have been approved as second-line treatments of metastatic cancers. However, no drug binding to the colchicine site has passed yet the trials required to become an approved anticancer drug, though this was the first druggable site described in tubulin.<sup>7</sup> Colchicine itself and the colchicine site ligand mebendazole are currently the only drugs used for the treatment of gout<sup>8</sup> and nematode infestation,<sup>9</sup> respectively.

Noscopine is a naturally occurring phthalideisoquinoline alkaloid obtained during opium harvesting.<sup>10</sup> It is used in humans as an oral antitussive agent.<sup>11</sup> The drug also displays a favorable toxicity profile and has been known for some time to act as a weak anticancer agent in certain *in vivo* models.<sup>12</sup> However, its molecular mechanism of action in this context is unknown. Like other microtubule targeting agents, noscopine arrests cells in the G2/M phase of the cycle at elevated concentrations (2  $\mu$ M), but it does not significantly alter microtubule formation *in vitro*.<sup>12,13</sup> Accordingly, the cellular effect could be caused by small amounts of an active contaminant or by metabolic activation of a prodrug. Strikingly, 7A *O*-demethylated noscopine derivatives (7A-hydroxy and 7A-amino derivatives) mirror the cellular phenotype of the parent

molecule but induce a G2/M arrest at about 500 times increased potency.<sup>14</sup> In a previous study, we suspected that the 7A-amino derivative of noscopine (7A-aminonoscopine) binds to the colchicine site of tubulin.<sup>13</sup> Tubulin inhibition through the colchicine site is a substoichiometric process<sup>15</sup> and involves blocking of the “curved to straight” conformational transition required for tubulin dimers to incorporate into the microtubule lattice.<sup>16</sup>

In this work, we performed an NMR-assisted docking process combining STD data and CORCEMA-ST calculations for the building of a 3D model that we further validated through the determination of the structure of the tubulin-7A-aminonoscopine complex by macromolecular crystallography. Our results enlighten the molecular mechanism of action of noscopine by suggesting that noscopine is a prodrug that requires an activation step via *O*-demethylation at its position 7A.

## RESULTS

**NMR-Directed Modeling of the Tubulin-7A-aminonoscopine Complex in Solution Indicates Binding to the Colchicine Site.** STD-NMR is a useful tool to investigate the interaction of small ligands with macromolecules. Aiming at understanding the lack of activity of noscopine on microtubule

Received: May 20, 2020

Published: July 13, 2020



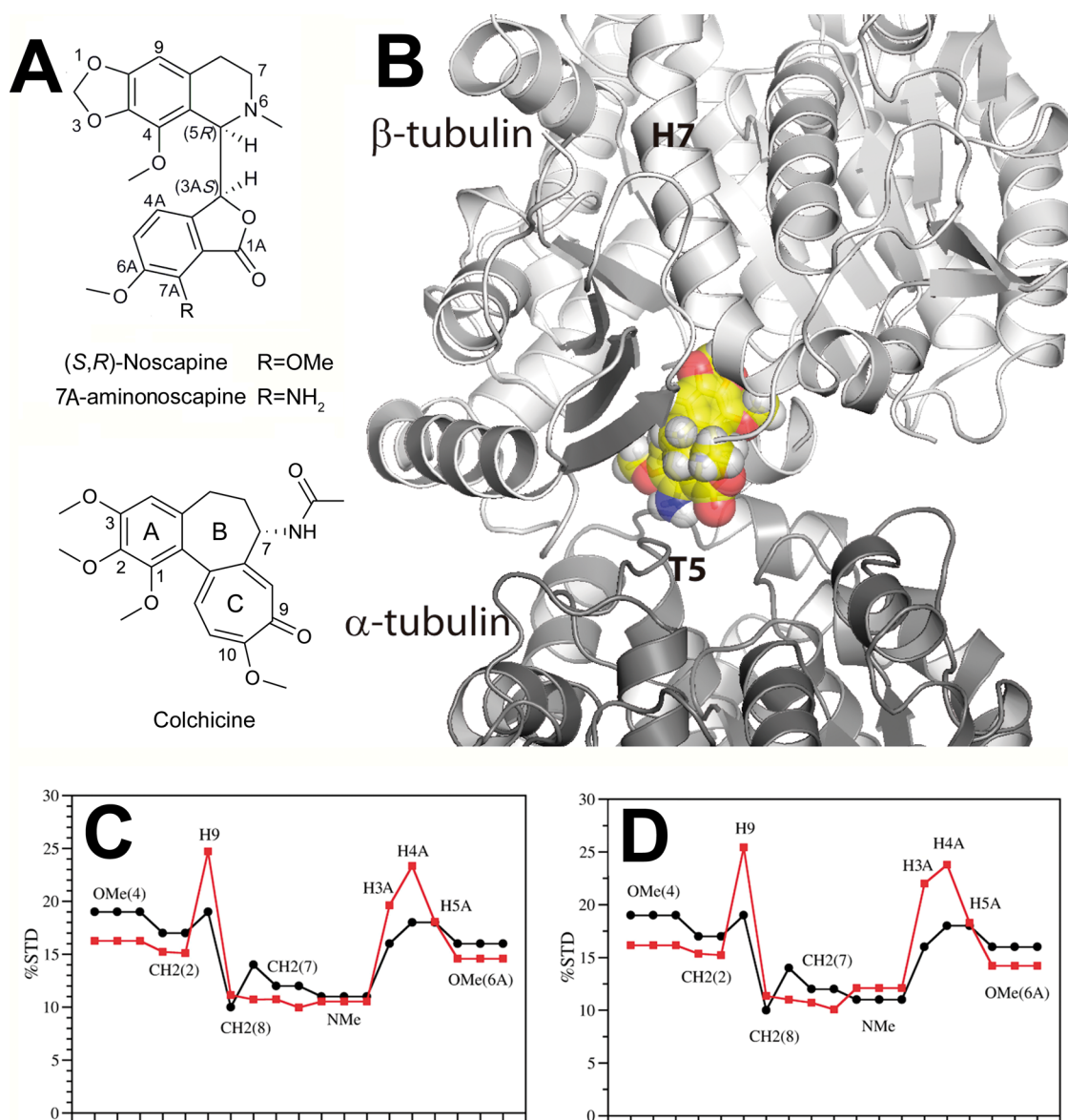


**Figure 1.** (A) Chemical structures of noscapine, 7A-aminonoscapine, and colchicine. (B) NMR-calculated binding pose of 7A-aminonoscapine (yellow) at the colchicine site of  $\beta_2$ -tubulin of the  $T_2R$  complex. (C, D) Experimental STD profiles (black line) of the tubulin-7A-aminonoscapine complex as compared with STD profiles calculated (red line) from the generated binding poses in the (C)  $\beta_1$ - and (D)  $\beta_2$ -tubulin subunits in the  $T_2R$ -TTL complex.

assembly and at unveiling the binding mode of 7A-aminonoscapine (Figure 1), we employed STD-NMR in combination with computational modeling. We further used the NMR STD and TR-NOESY data obtained previously<sup>13</sup> to model binding poses of 7A-aminonoscapine in the two tubulin dimers present in the  $T_2R$ -podophyllotoxin complex (PDB 1SA1).<sup>16</sup>

In agreement with the observed drug competition with the colchicine site ligand nocodazole,<sup>13</sup> the best binding poses with similar scores located to the colchicine sites of both tubulin dimers in the  $T_2R$  complex ( $\beta_1$ -tubulin, 0.16;  $\beta_2$ -tubulin, 0.18; Figure 1B). In both cases, nearly identical calculated STD profiles with rmsd values below 2 Å between them were revealed (Figure 1C,D). The calculated profiles were fully compatible with those experimentally determined, indicating that protons H9, H3A, and H4A of the ligand are closer to the protein surface and thus receive a larger saturation.

**High-Resolution Crystal Structure of the  $T_2R$ -TTL-7A-aminonoscapine Complex.** Despite noscapine showing a

weak colchicine-like activity, we were previously unable to detect any direct binding of the compound to the colchicine site using centrifugation- or spectroscopic-based assays.<sup>13</sup> Thus, the reason for the observed antitubulin activity of noscapine remains unknown.

Both NMR-determined poses (i.e., in  $\beta_1$ - and  $\beta_2$ -tubulin of the  $T_2R$  complex) revealed 7A-aminonoscapine in the same orientation, but its placement in the two binding sites is shifted with respect to each other (Figure S1), suggesting that the method does not have enough accuracy to understand the reason for noscapine's inability to bind the colchicine site. To investigate the structural reasons for the lack of activity of noscapine, we performed soaking experiments with noscapine and 7A-aminonoscapine using  $T_2R$ -TTL crystals obtained from a protein complex composed of two  $\alpha\beta$ -tubulin heterodimers, the stathmin-like protein RB3 and tubulin tyrosine ligase.<sup>17,18</sup> The  $T_2R$ -TTL system has successfully produced several structures of ligands bound to tubulin using X-ray crystallog-

raphy (reviewed in ref 19). The structure of T<sub>2</sub>R-TTL-7A-aminoscapine was solved at a 2.2 Å resolution, and we unequivocally found ligand density at the colchicine site (Figure 2A and Figure S2). Concomitantly, with the biochemical experiments,<sup>13</sup> we could not identify any extra density from crystals soaked with the parental noscapine (not shown).

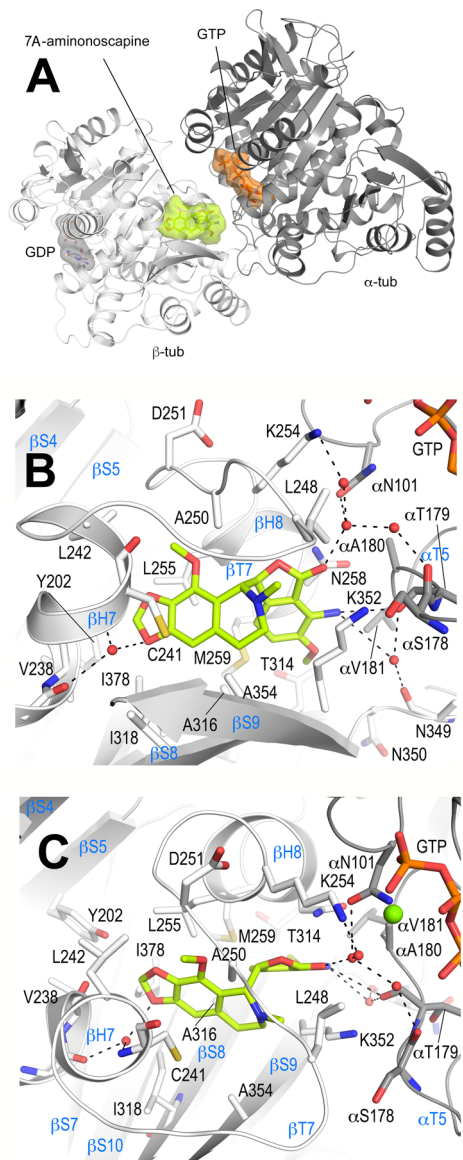


**Figure 2.** Overall tubulin-7A-aminoscapine complex structure. (A) Ribbon representation of the tubulin-bound 7A-aminoscapine on representation of the tubulin-bound 7A-aminoscapine structure (PDB ID 6Y6D). The  $\alpha$ - and  $\beta$ -tubulin chains are in dark and light gray, respectively. The ligand 7A-aminoscapine (light green) and the nucleotides (orange) are in sphere and stick representation, respectively. The carbon atoms of the individual nucleotides are colored according to their chain assignments. Oxygen and nitrogen atoms are colored in red and blue, respectively. (B, C) Close-up view of the atomic interaction network observed between 7A-aminoscapine (light green) and tubulin (gray) in two different orientations. Interacting residues of tubulin are shown in a stick representation and are labeled. Oxygen and nitrogen atoms are colored in red and blue, respectively. Hydrogen bonds are depicted as black dashed lines. Secondary structural elements of tubulin are labeled in blue. For simplicity, only  $\alpha$ -tubulin residues are indicated with an “ $\alpha$ ”.

The ligand in the colchicine site occupies a similar space as colchicine (Figure 3A). Noticeably, the conformation of 7A-

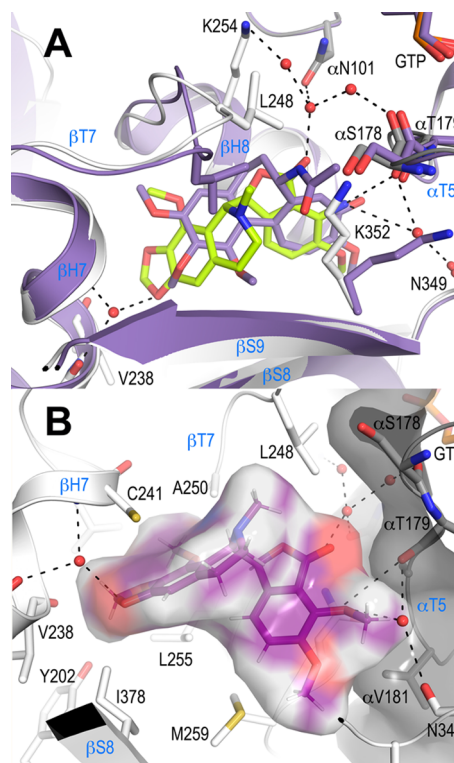


**Figure 3.** (A) Superposition of the tubulin-7A-aminoscapine (light green, PDB ID 6Y6D) and tubulin-colchicine (slate, PDB ID 4O2B) complex structures. The structures were superimposed onto the  $\beta$ 1-tubulin of their respective T<sub>2</sub>R-TTL complexes. Interacting residues of tubulin discussed in the text are shown in stick representation and are labeled. Oxygen and nitrogen atoms are colored in red and blue, respectively. Hydrogen bonds are depicted as black dashed lines. Secondary structural elements of tubulin are labeled in blue. (B) Modeled noscapine molecule into the crystallographic determined 7A-aminoscapine binding site, highlighting how the 7A-methoxy group would clash into the  $\alpha$ T5-loop. The clash is in agreement with the calculated NMR model and suggests why noscapine does not bind to tubulin.

aminoscapine using either NMR or crystallography is similar with an rmsd of 0.18 Å in  $\beta$ 2-tubulin (Figure S1A), while the NMR-calculated pose is displaced from the actual crystallographic one in  $\beta$ 1-tubulin (Figure S1B). The overall structure of tubulin in the T<sub>2</sub>R-TTL-7A-aminoscapine complex superimposed well with that of the ligand free complex structure<sup>18</sup> with an overall rmsd of 0.29 Å over 1996 C $_{\alpha}$ -atoms and a  $\beta$ -tubulin rmsd of 0.14 Å over 365 C $_{\alpha}$ -atoms, suggesting that the binding of 7A-aminoscapine does not affect the conformation of tubulin.

The three-membered [1,3]dioxolo-isoquinoline ring of 7A-aminoscapine is stacked between the side chains of  $\beta$ Cys241 of helix  $\beta$ H7 and  $\beta$ Leu255 of helix  $\beta$ H8 (Figure 3B,C). The dioxolo moiety points into the pocket shaped by the side chains of  $\beta$ Tyr202,  $\beta$ Val238,  $\beta$ Leu242,  $\beta$ Leu255,  $\beta$ Ile318, and  $\beta$ Ile378, and the oxygen O1 forms two water-mediated H-bonds to both the main chain carbonyl of  $\beta$ Gly237 and the main chain amide of  $\beta$ Cys241 of helix  $\beta$ H7. The N6-methyl group is equatorially oriented toward the nucleotide N-site of  $\alpha$ -tubulin; however, it does not engage in electrostatic interactions with the nucleotide.

The protonated N6 points toward the side chain of  $\beta$ Cys241 and may engage in a weak interaction with the lone pairs of the sulfhydryl group (4.9 Å distance). The 4-methoxy moiety forms a hydrophobic contact with the side chains of  $\beta$ Leu242 and  $\beta$ Ala250. The benzofuran-1-one moiety is stacked between the side chains of  $\beta$ Asn258 and  $\beta$ Lys352, and its 1A-carbonyl forms water-mediated H-bonds to the side chains of  $\alpha$ Asn101 and  $\beta$ Lys254 and to the main chain carbonyl of  $\alpha$ Ser178. The 7A-amino group points toward the tubulin intradimer interface and is in direct and water-mediated H-bond contact to both the main chain carbonyls of  $\alpha$ Thr179 and  $\beta$ Asn349. The 6A-methoxy moiety occupies the cavity shaped by the carboxy-terminal end of helix  $\beta$ H8, the amino-terminal end of strand  $\beta$ S9, and the  $\alpha$ Val181 side chain on the  $\alpha$ T5-loop.

The tubulin-colchicine and tubulin-7A-aminonoscapiene structures superimpose very well (overall rmsd of 0.16 Å over 1882  $C_{\alpha}$ -atoms and a  $\beta$ -tubulin rmsd of 0.14 Å over 328  $C_{\alpha}$ -atoms; Figure 3A). The 7A-amino and the 6A-methoxy moieties of the benzofuran-1-one ring occupy almost the same space as the corresponding carbonyl and methoxy groups of the C-ring of colchicine, thereby establishing similar polar and hydrophobic contacts. Compared to both the colchicine-bound and the apo-tubulin state, the equatorial N6-methyl group of 7A-aminonoscapiene displaces the side chain of  $\beta$ Leu247, thereby causing a flip of the  $\beta$ T7-loop. The  $\beta$ Lys352 side chain is flipped toward the ligand and occupies the space that is otherwise filled by the 7-acetamide moiety of colchicine. Overall, these structural similarities suggest that both ligands most likely perturb tubulin by a similar mechanism, i.e., by preventing the curved to straight conformational transition required for tubulin assembly into microtubules.<sup>20</sup>

## DISCUSSION AND CONCLUSIONS

Our high-resolution crystal structure confirms that 7A-aminonoscapiene targets the colchicine site of tubulin (Figure 2). This result corroborates that the inhibitory effects of noscapine derivatives on tubulin assembly into microtubules, and the subsequent cellular effects<sup>13,14</sup> are exerted using the same molecular mechanism as colchicine. Based on our structural information, we can now explain the lack of noscapine's activity *in vitro* and the activity improvement of some developed derivatives. The 7A-methoxy group in noscapine clashes with the  $\alpha$ T5-loop of tubulin, precluding noscapine binding to the colchicine site (Figure 3B). The reduction of the noscapine lactone produced cyclic ether noscapinoids with increased activity,<sup>21</sup> which could be explained by the loss of the H-bond network established by the 1A-carbonyl group with  $\alpha$ -tubulin; it would also allow for a better accommodation of the 7A-methoxy group within the pocket. The best cellular toxicity activities were obtained with 9-halogenated derivatives,<sup>22</sup> which likely display increased contacts with strands S8–S9 in  $\beta$ -tubulin. Otherwise, *N*-substituted 6'-derivatives showed different effects on the inhibition of cell proliferation,<sup>21</sup> which could be explained by the interaction of the different moieties with the  $\beta$ T7-loop. Finally, bulkier substitutes at the 7A-position showed better activities than noscapine.<sup>23</sup> The most reasonable explanation for those results is that derivatives containing such substitutes bind tubulin in a different way.

An immediate question emerging from these observations is the following: from where does the colchicine-like activity observed for the parental noscapine come from? We hypothesize that the observed *in vivo* activity of noscapine is the result of its metabolic bioactivation. A prodrug is a molecule with a low or

neglectable activity against a pharmacological target as compared with one of its metabolites.<sup>24</sup> In humans, the metabolism of xenobiotics is mostly related with cytochrome P450 enzymes that, among other activities, perform the oxidation of a carbon group bound to oxygen or other heteroatoms.<sup>25</sup> This reaction leads to the release of the carbon and leaves an alcohol, amine, or thiol in the molecule,<sup>25</sup> which is a common mechanism for the release of a drug from its prodrug.<sup>24</sup> For instance, morphine or norcodeine are the consequence of *O*-demethylation and *N*-demethylation of codein, respectively.<sup>26</sup> In fact, the oxidation mechanism is a common way of antitumoral prodrug activation (e.g., cyclophosphamide,<sup>27</sup> dacarbazine,<sup>28</sup> and tamoxifen<sup>29</sup>) where the hepatic CYP2D6 enzyme is mostly involved in the activation process, as exemplified by codeine and tamoxifen.<sup>24</sup>

The noscapine metabolism is well understood and includes an extensive "first pass" metabolism in rats, rabbits, and humans mainly by C–C cleavage, *O*-demethylation, and cleavage of the methylenedioxy group.<sup>30–32</sup> The metabolic map of noscapine has been extensively characterized by Fang et al.<sup>32</sup> This study shows that the 7A-demethylated product is one of the major metabolites of noscapine in cells and *in vivo* after being processed by CYP3A5. The same metabolite was also identified in mice both unmodified and as its glucuronide after being processed by UGT1A1/3/9. The 7A-demethylated product of noscapine is a tubulin assembly inhibitor that is as potent as vinblastine, showing an  $IC_{50}$  of 0.6  $\mu$ M in A549 cells.<sup>14</sup> Considering that the noscapine doses effective for tumor inhibition in mice are 120 mg/kg,<sup>12</sup> while the dose of colchicine (when used as an antitumor drug) is about 4000 times lower (i.e. 30  $\mu$ g/kg<sup>33</sup>), it is reasonable to assume that only a small fraction of the metabolically processed 7A-desmethylated noscapine derivative is required to justify the observed activity.

In conclusion, we propose that noscapine's cytotoxicity is a consequence of the oxidation of its methoxy carbon at position 7A, which leads to the formation of the active phenol. The resulting drug is then able to bind tubulin and block microtubule assembly in a colchicine-like manner.<sup>13</sup>

## EXPERIMENTAL SECTION

**Proteins and Ligands.** Purified calf brain tubulin and chemicals were obtained, as previously described.<sup>34,35</sup> Noscapine was from Merck. 7A-Aminonoscapiene (Figure 1) was synthesized, as described.<sup>14</sup> The compounds were diluted in 99.8%  $d_6$ -DMSO (Merck) to a final concentration of 20 mM and stored at  $-20$  °C.

**NMR-Directed Structure Modeling.** The structure of the 7A-aminonoscapiene-tubulin complex was modeled using molecular docking based on NMR-STD measurements.<sup>36</sup> We employed the NMR-STD spectra of 7A-aminonoscapiene bound to tubulin previously obtained; the coordinates of the 7A-aminonoscapiene bound to the protein (obtained from TR-NOESY measurements)<sup>13</sup> and the structure of tubulin in the T<sub>2</sub>R-podophyllotoxin-tubulin complex (pdb: 1SA1)<sup>16</sup> after removing podophyllotoxin from the binding site.

Prior to use, the structures were optimized using Polak–Ribiere conjugated gradient (PRCG) and implemented in MacroModel,<sup>37</sup> employing an OPLS2005 force field.<sup>38–40</sup> Water solvation was implicitly considered following a generalized Born model GB/SA.<sup>41</sup> Cutoff distances for the van der Waals potential were 8.0 Å, while those for the electrostatic potential were 20.0 Å. The maximum number of iterations was set to 9000, while the minimization was considered finished when the energy gradient was smaller than 0.05 kJ/mol Å<sup>-1</sup>.

We generated the complex structure by iterative fitting of the STD spectrum calculated from generated binding poses to the experimentally determined STD spectrum. To do so, we calculated tens of binding poses employing AutoDock Vina<sup>42</sup> within a defined area of the

protein surface, which was considered rigid. In this work, a 25 Å parallelepiped build around  $\beta$ 1- and  $\beta$ 2-tubulin cavities was employed, and 20 poses were generated per cavity. The theoretical STD spectrum of 7A-aminoscapine bound to tubulin was calculated for each binding pose using the CORCEMA-ST matlab routine.<sup>43,44</sup> For these full relaxation matrix calculations, an order parameter  $S^2 = 0.85$  was employed to account for the fast rotation of the methyl groups, as implemented in CORCEMA-ST. For each generated pose, the apparent binding and association constants ( $K_b^{\text{app}}$  and  $k_{\text{on}}^{\text{app}}$ ) and the rotational correlation time of the free  $\tau_c^{\text{f,app}}$  and bound  $\tau_c^{\text{b,app}}$  compound were optimized to minimize the difference between the calculated and the measured STD spectrum. The best binding poses were selected and sorted according to their difference with the experimental STD spectrum. The structure with the best score was found in the colchicine site employing the following parameters:  $K_b^{\text{app}} 1 \pm 0.5 \times 10^5 \text{ M}^{-1}$ ,  $k_{\text{on}}^{\text{app}} 1 \pm 0.5 \times 10^6 \text{ M}^{-1} \text{ s}^{-1}$ ,  $\tau_c^{\text{f,app}} 0.8 \pm 0.3 \text{ ns}$ , and  $\tau_c^{\text{b,app}} 100 \pm 50$  (for site  $\beta$ 1) or  $80 \pm 5$  (for site  $\beta$ 2) ns.

**Crystallization, Data Collection, and Structure Determination.** Crystals of T<sub>2</sub>R-TTL were grown, as described by Protá et al.<sup>17,18</sup> Briefly, the T<sub>2</sub>R-TTL complex was crystallized by the vapor diffusion method at 20 °C using the microseeding technique. Crystals grew for over 2 days in precipitant solution consisting of 5% PEG 4 K, 11% glycerol, 30 mM MgCl<sub>2</sub>, 30 mM CaCl<sub>2</sub>, and 100 mM MES/imidazole, pH 6.5. The crystals were soaked overnight at 20 °C in reservoir solutions containing 2 mM 7A-aminoscapine and subsequently flash-cooled in liquid nitrogen upon two consecutive transfers to reservoir solutions containing (i) 10% PEG 4 K and 16% glycerol and (ii) 10% PEG 4 K and 20% glycerol. Native data were collected at 100 K at beamline X06DA of the Swiss Light Source (Paul Scherrer Institut, Villigen PSI, Switzerland). Data were processed and merged with XDS<sup>45</sup> to 2.2 Å resolution.

The T<sub>2</sub>R-TTL-7A-aminoscapine structure was determined by the difference Fourier method using the phases of the T<sub>2</sub>R-TTL complex (PDB ID 4I4T) in the absence of ligands and solvent molecules as a starting point for refinement. After three cycles of rigid body and subsequent three cycles of restrained refinement in Phenix,<sup>46</sup> clear difference density delineating the shape of a bound molecule to the colchicine site was visible.

After correction of geometry, Ramachandran, and rotamer outliers, missing water molecules were added to the model, and additional cycles of restrained refinement in Phenix<sup>46</sup> were performed. The 7A-aminoscapine molecule was then placed into the difference electron density map at the colchicine site, and the model was further improved by iterative rounds of model building and refinement. The final model was refined to 2.2 Å resolution with crystallographic *R* values of 18.4% (*R*<sub>work</sub>) and 22.4% (*R*<sub>free</sub>). The model has good geometry with small root-mean-square deviations (rmsd) from ideal values for bond lengths and bond angles. The quality of the structures was assessed with MolProbity.<sup>47</sup> Data collection and refinement statistics are given in Table S1. Molecular graphics and analyses were performed with PyMol (the PyMOL Molecular Graphics System, Version 1.8.6.2. Schrödinger, LLC).

## ■ ASSOCIATED CONTENT

### Supporting Information

The Supporting Information is available free of charge at <https://pubs.acs.org/doi/10.1021/acs.jmedchem.0c00855>.

Data collection and refinement statistics of the crystallographic analysis (Table S1), comparison between crystal and NMR structures (Figure S1), and the omit map of tubulin-bound 7A-aminoscapine (Figure S2) (PDF)

NMR models of the T<sub>2</sub>R-TTL-7-demethoxy-amino noscapine complexes (PDB, PDB)

Molecular formula strings (CSV)

## ■ AUTHOR INFORMATION

### Corresponding Author

J. Fernando Díaz – Centro de Investigaciones Biológicas Margarita Salas-CSIC, 28040 Madrid, Spain; [orcid.org/0000-0003-2743-3319](https://orcid.org/0000-0003-2743-3319); Email: [fer@cib.csic.es](mailto:fer@cib.csic.es)

### Authors

María A. Oliva – Centro de Investigaciones Biológicas Margarita Salas-CSIC, 28040 Madrid, Spain

Andrea E. Protá – Laboratory of Biomolecular Research, Division of Biology and Chemistry, Paul Scherrer Institut, CH-5232 Villigen PSI, Switzerland

Javier Rodríguez-Salarichs – Centro de Investigaciones Biológicas Margarita Salas-CSIC, 28040 Madrid, Spain

Youssef L. Bennani – adMare Bio Innovations, Centre d'innovation NÉOMED, Montréal, Quebec H4S 1Z9, Canada

Jesús Jiménez-Barbero – CIC bioGUNE, Basque Research Technology Alliance (BRTA), 48170 Derio, Spain; Ikerbasque, Basque Foundation for Science, Bilbao 48009, Spain; Department of Organic Chemistry II, Faculty of Science & Technology, University of the Basque Country, 48940 Leioa, Bizkaia, Spain; [orcid.org/0000-0001-5421-8513](https://orcid.org/0000-0001-5421-8513)

Katja Bargsten – Laboratory of Biomolecular Research, Division of Biology and Chemistry, Paul Scherrer Institut, CH-5232 Villigen PSI, Switzerland

Ángeles Canales – Departamento Química Orgánica I, Facultad Ciencias Químicas, Universidad Complutense de Madrid, 28040 Madrid, Spain; [orcid.org/0000-0003-0542-3080](https://orcid.org/0000-0003-0542-3080)

Michel O. Steinmetz – Laboratory of Biomolecular Research, Division of Biology and Chemistry, Paul Scherrer Institut, CH-5232 Villigen PSI, Switzerland; University of Basel, Basel CH-4056, Switzerland; [orcid.org/0000-0001-6157-3687](https://orcid.org/0000-0001-6157-3687)

Complete contact information is available at:

<https://pubs.acs.org/doi/10.1021/acs.jmedchem.0c00855>

### Author Contributions

¶M.A.O., A.E.P., and J.R.-S. contributed equally.

### Notes

The authors declare no competing financial interest.

The PDB code for the crystallographic structure of the T<sub>2</sub>R-TTL-7-demethoxy-amino noscapine complex is 6Y6D.

## ■ ACKNOWLEDGMENTS

We thank Ganadería Fernando Díaz for calf brains supply and staff of beamline X06DA of the Swiss Light Source (Paul Scherrer Institut, Villigen PSI, Switzerland) for their support. This work was supported by Ministerio de Ciencia e Innovación PID2019-104545RB-I00 and Fondo de Investigaciones Sanitarias COV20-01007 to J.F.D., CTQ2016-76263-P to A.C., the Swiss National Science Foundation (31003A\_166608) to M.O.S., H2020-MSCA-ITN-2019 860070 TUBINTRAIN to A.E.P. and J.F.D., and a donation from Club deportivo Escuela Hungarosa de Pontevedra.

## ■ ABBREVIATIONS

CORCEMA-ST, complete relaxation and conformational exchange matrix analysis of saturation transfer; STD, saturation transfer difference; TTL-T<sub>2</sub>R, bovine brain  $\alpha\beta$ -tubulin, rat stathmin-like protein RB3, and chicken tubulin-tyrosine ligase complex; TR-NOESY, two-dimensional transferred nuclear Overhauser effect spectroscopy

## REFERENCES

- (1) Johnson, I. S.; Armstrong, J. G.; Gorman, M.; Burnett, J. P. The Vinca Alkaloids: A New Class of Oncolytic Agents. *Cancer Res.* **1963**, *23*, 1390–1427.
- (2) Donehower, R. C. The Clinical Development of Paclitaxel: A Successful Collaboration of Academia, Industry and the National Cancer Institute. *Oncologist* **1996**, *1*, 240–243.
- (3) Prota, A. E.; Bargsten, K.; Diaz, J. F.; Marsh, M.; Cuevas, C.; Liniger, M.; Neuhaus, C.; Andreu, J. M.; Altmann, K. H.; Steinmetz, M. O. A new Tubulin-binding Site and Pharmacophore for Microtubule-stabilizing Anticancer Drugs. *Proc. Natl. Acad. Sci. U. S. A.* **2014**, *111*, 13817–13821.
- (4) Lambert, J. M.; Chari, R. V. J. Ado-trastuzumab Emtansine (T-DM1): An Antibody–Drug Conjugate (ADC) for HER2-Positive Breast Cancer. *J. Med. Chem.* **2014**, *57*, 6949–6964.
- (5) Doodhi, H.; Prota, A. E.; Rodríguez-García, R.; Xiao, H.; Custar, D. W.; Bargsten, K.; Katrukha, E. A.; Hilbert, M.; Hua, S.; Jiang, K.; Grigoriev, I.; Yang, C.-P. H.; Cox, D.; Horwitz, S. B.; Kapitein, L. C.; Akhmanova, A.; Steinmetz, M. O. Termination of Protofilament Elongation by Eribulin Induces Lattice Defects that Promote Microtubule Catastrophes. *Curr. Biol.* **2016**, *26*, 1713–1721.
- (6) Denduluri, N.; Swain, S. M. Ixabepilone for the Treatment of Solid Tumors: a Review of Clinical Data. *Expert Opin. Invest. Drugs* **2008**, *17*, 423–435.
- (7) Borisy, G. G.; Taylor, E. W. The Mechanism of Action of Colchicine. Binding of Colchicine-3H to Cellular Protein. *J. Cell Biol.* **1967**, *34*, 525–533.
- (8) Khanna, D.; Khanna, P. P.; Fitzgerald, J. D.; Singh, M. K.; Bae, S.; Neogi, T.; Pillinger, M. H.; Merrill, J.; Lee, S.; Prakash, S.; Kaldas, M.; Gogia, M.; Perez-Ruiz, F.; Taylor, W.; Lioté, F.; Choi, H.; Singh, J. A.; Dalbeth, N.; Kaplan, S.; Niyyar, V.; Jones, D.; Yarows, S. A.; Roessler, B.; Kerr, G.; King, C.; Levy, G.; Furst, D. E.; Edwards, N. L.; Mandell, B.; Schumacher, H. R.; Robbins, M.; Wenger, N.; Terkeltaub, R. 2012 American College of Rheumatology Guidelines for Management of Gout. Part 2: Therapy and Antiinflammatory Prophylaxis of Acute Gouty Arthritis. *Arthritis Care Res.* **2012**, *64*, 1447–1461.
- (9) Lacey, E. Mode of Action of Benzimidazoles. *Parasitol. Today* **1990**, *6*, 112–115.
- (10) Warolin, C. Pierre-Jean Robiquet (Rennes, 14 janvier 1780-Paris, 29 avril 1840). *Rev. Hist. Pharm.* **1999**, 97–110.
- (11) Singh, H.; Singh, P.; Kumari, K.; Chandra, A.; K Dass, S.; Chandra, R. A Review on Noscaphine, and its Impact on Heme Metabolism. *Curr. Drug Metab.* **2013**, *14*, 351–360.
- (12) Ye, K.; Ke, Y.; Keshava, N.; Shanks, J.; Kapp, J. A.; Tekmal, R. R.; Petros, J.; Joshi, H. C. Opium Alkaloid Noscaphine is an Antitumor Agent that Arrests Metaphase and induces Apoptosis in Dividing Cells. *Proc. Natl. Acad. Sci. U. S. A.* **1998**, *95*, 1601–1606.
- (13) Bennani, Y. L.; Gu, W.; Canales, A.; Díaz, J. F.; Eustace, B. K.; Hoover, R. R.; Jiménez-Barbero, J.; Nezami, A.; Wang, T. Tubulin Binding, Protein-Bound Conformation in Solution, and Antimitotic Cellular Profiling of Noscaphine and Its Derivatives. *J. Med. Chem.* **2012**, *55*, 1920–1925.
- (14) Anderson, J. T.; Ting, A. E.; Boozer, S.; Brunden, K. R.; Crumrine, C.; Danzig, J.; Dent, T.; Faga, L.; Harrington, J. J.; Hodnick, W. F.; Murphy, S. M.; Pawlowski, G.; Perry, R.; Raber, A.; Rundlett, S. E.; Stricker-Krongrad, A.; Wang, J.; Bennani, Y. L. Identification of Novel and Improved Antimitotic Agents Derived from Noscaphine. *J. Med. Chem.* **2005**, *48*, 7096–7098.
- (15) Perez-Ramirez, B.; Andreu, J. M.; Gorbunoff, M. J.; Timasheff, S. N. Stoichiometric and Substoichiometric Inhibition of Tubulin Self-Assembly by Colchicine Analogues. *Biochemistry* **1996**, *35*, 3277–3285.
- (16) Ravelli, R. B. G.; Gigant, B.; Curmi, P. A.; Jourdain, I.; Lachkar, S.; Sobel, A.; Knossow, M. Insight into Tubulin Regulation from a Complex with Colchicine and a Stathmin-like Domain. *Nature* **2004**, *428*, 198–202.
- (17) Prota, A. E.; Bargsten, K.; Zurwerra, D.; Field, J. J.; Díaz, J. F.; Altmann, K.-H.; Steinmetz, M. O. Molecular Mechanism of Action of Microtubule-Stabilizing Anticancer Agents. *Science* **2013**, *339*, 587–590.
- (18) Prota, A. E.; Magiera, M. M.; Kuijpers, M.; Bargsten, K.; Frey, D.; Wieser, M.; Jaussi, R.; Hoogenraad, C. C.; Kammerer, R. A.; Janke, C.; Steinmetz, M. O. Structural Basis of Tubulin Tyrosination by Tubulin Tyrosine Ligase. *J. Cell Biol.* **2013**, *200*, 259–270.
- (19) Steinmetz, M. O.; Prota, A. E. Microtubule-Targeting Agents: Strategies To Hijack the Cytoskeleton. *Trends Cell Biol.* **2018**, 776–792.
- (20) Buey, R. M.; Díaz, J. F.; Andreu, J. M. The Nucleotide Switch of Tubulin and Microtubule Assembly: a Polymerization-driven Structural Change. *Biochemistry* **2006**, *45*, 5933–5938.
- (21) DeBono, A. J.; Xie, J. H.; Ventura, S.; Pouton, C. W.; Capuano, B.; Scammells, P. J. Synthesis and Biological Evaluation of N-Substituted Noscaphine Analogues. *ChemMedChem* **2012**, *7*, 2122–2133.
- (22) Aneja, R.; Vangapandu, S. N.; Lopus, M.; Visweswarappa, V. G.; Dhiman, N.; Verma, A.; Chandra, R.; Panda, D.; Joshi, H. C. Synthesis of Microtubule-Interfering Halogenated Noscaphine Analogs that perturb Mitosis in Cancer Cells followed by Cell Death. *Biochem. Pharmacol.* **2006**, *72*, 415–426.
- (23) Mishra, R. C.; Karna, P.; Gundala, S. R.; Pannu, V.; Stanton, R. A.; Gupta, K. K.; Robinson, M. H.; Lopus, M.; Wilson, L.; Henary, M.; Aneja, R. Second Generation Benzofuranone Ring substituted Noscaphine Analogs: Synthesis and Biological Evaluation. *Biochem. Pharmacol.* **2011**, *82*, 110–121.
- (24) Ortiz de Montellano, P. R. Cytochrome P450-activated Prodrugs. *Future Med. Chem.* **2013**, *5*, 213–228.
- (25) Anzenbacher, P.; Anzenbacherová, E. Cytochromes P450 and Metabolism of Xenobiotics. *Cell. Mol. Life Sci.* **2001**, *58*, 737–747.
- (26) Sindrup, S. H.; Brøsen, K. The Pharmacogenetics of Codeine Hypoalgesia. *Pharmacogenet. Genom.* **1995**, *5*, 335–346.
- (27) Friedman, O. M.; Wodinsky, I.; Myles, A. Cyclophosphamide (NSC-26271)-related Phosphoramidate Mustards- Recent Advances and Historical Perspective. *Cancer Treat Rep* **1976**, *60*, 337–346.
- (28) Marchesi, F.; Turriziani, M.; Tortorelli, G.; Avvisati, G.; Torino, F.; De Vecchis, L. Triazene Compounds: Mechanism of Action and Related DNA Repair Systems. *Pharmacol. Res.* **2007**, *56*, 275–287.
- (29) Desta, Z.; Ward, B. A.; Soukhova, N. V.; Flockhart, D. A. Comprehensive Evaluation of Tamoxifen Sequential Biotransformation by the Human Cytochrome P450 System in Vitro: Prominent Roles for CYP3A and CYP2D6. *J. Pharmacol. Exp. Ther.* **2004**, *310*, 1062–1075.
- (30) Tsunoda, N.; Yoshimura, H. Metabolic Fate of Noscaphine; III. Further Studies on Identification and Determination of the Metabolites. *Xenobiotica* **1981**, *11*, 23–32.
- (31) Tsunoda, N.; Yoshimura, H. Metabolic Fate of Noscaphine. II. Isolation and identification of Novel Metabolites produced by C–C bond Cleavage. *Xenobiotica* **1979**, *9*, 181–187.
- (32) Fang, Z.-Z.; Krausz, K. W.; Li, F.; Cheng, J.; Tanaka, N.; Gonzalez, F. J. Metabolic Map and Bioactivation of the anti-Tumour Drug Noscaphine. *Br. J. Pharmacol.* **2012**, *167*, 1271–1286.
- (33) Slobodnick, A.; Shah, B.; Krasnokutsky, S.; Pillinger, M. H. Update on Colchicine, 2017. *Rheumatology Oxford* **2018**, *57*, i4–i11.
- (34) Diaz, J. F.; Andreu, J. M. Assembly of Purified GDP-Tubulin into Microtubules induced by Taxol and Taxotere: Reversibility, Ligand Stoichiometry, and Competition. *Biochemistry* **1993**, *32*, 2747–2755.
- (35) Andreu, J. M. Large Scale Purification of Brain Tubulin. In *Methods Mol. Biol.*, Zhou, J., Ed. Humana Press Inc.: Totowa, NJ, 2007; Vol. 137, pp 17–28.
- (36) Rodríguez-Salarichs, J.; Canales, A.; Diaz, J. F. Ph.D. Thesis: Desarrollo y Validación Experimental de un Método para la Obtención de Estructuras de Complejos Ligando/Receptor basado en Resonancia Magnética Nuclear. 2017.
- (37) Mohamadi, F.; Richards, N. G. J.; Guida, W. C.; Liskamp, R.; Lipton, M.; Caufield, C.; Chang, G.; Hendrickson, T.; Still, W. C. MacroModel an Integrated Software System for Modeling Organic and Bioorganic Molecules using Molecular Mechanics. *J. Comput. Chem.* **1990**, *11*, 440–467.

(38) Jorgensen, W. L.; Tiradorives, J. The OPLS Potential Functions for Proteins - Energy Minimizations for Crystals of Cyclic-peptides and Crambin. *JACS* **1988**, *110*, 1657–1666.

(39) Kaminski, G. A.; Friesner, R. A.; Tirado-Rives, J.; Jorgensen, W. L. Evaluation and Reparametrization of the OPLS-AA Force Field for Proteins via Comparison with Accurate Quantum Chemical Calculations on Peptides. *J. Phys. Chem. B* **2001**, *105*, 6474–6487.

(40) Bertelsen, L. B.; Shen, Y. Y.; Nielsen, T.; Stodkilde-Jorgensen, H.; Lloyd, G. K.; Siemann, D. W.; Horsman, M. R. Vascular Effects of Plinabulin (NPI-2358) and the Influence on Tumour Response when given alone or combined with Radiation. *Int. J. Radiat. Biol.* **2011**, *87*, 1126–1134.

(41) Still, W. C.; Tempczyk, A.; Hawley, R. C.; Hendrickson, T. Semianalytical Treatment of Solvation for Molecular Mechanics and Dynamics. *J. Am. Chem. Soc.* **1990**, *112*, 6127–6129.

(42) Trott, O.; Olson, A. J. AutoDock Vina: improving the Speed and Accuracy of Docking with a new Scoring Function, Efficient Optimization, and Multithreading. *J. Comput. Chem.* **2010**, *31*, 455–461.

(43) Moseley, H. N. B.; Curto, E. V.; Krishna, N. R. Complete Relaxation and Conformational Exchange Matrix (CORCEMA) Analysis of NOESY Spectra of Interacting Systems - 2-Dimensional Transferred NOESY. *J. Magn. Reson., Ser. B* **1995**, *108*, 243–261.

(44) Jayalakshmi, V.; Krishna, N. R. Complete Relaxation and Conformational Exchange Matrix (CORCEMA) Analysis of Intermolecular Saturation Transfer Effects in Reversibly forming Ligand-Receptor Complexes. *J. Magn. Reson.* **2002**, *155*, 106–118.

(45) Kabsch, W. XDS. *Acta Crystallogr. Sect. D* **2010**, *66*, 125–132.

(46) Adams, P. D.; Afonine, P. V.; Bunkóczy, G.; Chen, V. B.; Davis, I. W.; Echols, N.; Headd, J. J.; Hung, L.-W.; Kapral, G. J.; Grosse-Kunstleve, R. W.; McCoy, A. J.; Moriarty, N. W.; Oeffner, R.; Read, R. J.; Richardson, D. C.; Richardson, J. S.; Terwilliger, T. C.; Zwart, P. H. PHENIX: a Comprehensive Python-based System for Macromolecular Structure Solution. *Acta Crystallogr. Sect. D* **2010**, *66*, 213–221.

(47) Chen, V. B.; Arendall, W. B., III; Headd, J. J.; Keedy, D. A.; Immormino, R. M.; Kapral, G. J.; Murray, L. W.; Richardson, J. S.; Richardson, D. C. MolProbity: all-Atom Structure Validation for Macromolecular Crystallography. *Acta Crystallogr. Sect. D* **2010**, *66*, 12–21.